Published in final edited form as:
Nat Chem. 2018 December ; 10(12): 1234–1245. doi:10.1038/s41557-018-0144-2.

Mining the cellular inventory of pyridoxal phosphate-dependent enzymes with functionalized cofactor mimics

Annabelle Hoegl, **Matthew B. Nodwell**, **Volker C. Kirsch**, **Nina C. Bach**, **Martin Pfanzelt**, **Matthias Stahl**, **Sabine Schneider**, and **Stephan A. Sieber***
Department of Chemistry, Center for Integrated Protein Science Munich (CIPSM), Technische Universität München, Lichtenbergstraße 4, 85747 Garching, Germany

Abstract

Pyridoxal phosphate (PLP) is an enzyme cofactor required for the chemical transformation of biological amines in numerous essential cellular processes. PLP-dependent enzymes (PLP-DEs) are ubiquitous and evolutionarily diverse, making their classification based on sequence homology challenging. Here we present a chemical proteomic method for reporting on PLP-DEs using functionalized cofactor probes. We synthesized pyridoxal (PL)-analogues modified at the 2'-position which are taken up by cells and metabolized in situ. These PL-analogues are phosphorylated to functional cofactor surrogates by cellular PL kinases and bind to PLP-DEs via an aldimine bond which can be rendered irreversible by $NaBH_4$ reduction. Conjugation to a reporter tag enables the subsequent identification of PLP-DEs using quantitative, label-free mass spectrometry. Using these probes we accessed a significant portion of the *Staphylococcus aureus* PLP-DE proteome (73%) and annotate uncharacterized proteins as novel PLP-DEs. We also show that this approach can be used to study structural tolerance within PLP-DE active sites and to screen for off-targets of the PLP-DE inhibitor D-cycloserine.

Pyridoxal phosphate (PLP), a bioactive component of vitamin B_6, is a versatile enzyme cofactor that facilitates diverse chemical transformations of biological amines.1–3 PLP-dependent enzymes (PLP-DEs) constitute a ubiquitous family of biocatalysts that are widely

*Correspondence and requests for materials should be addressed to S.A.S. stephan.sieber@tum.de.

Author Contributions
A.H., M.B.N. and S.A.S. conceived and designed the project. A.H., M.B.N. and M.P. synthesized PL-probes. A.H., M.B.N. and M.P. conducted biochemical characterization of probes and PLP-DEs including purification of recombinant proteins, enzyme kinetics assays, UV-Vis measurements and *in vitro* protein labeling experiments (MS and gel-based). S.S. performed crystallization and determined X-ray structures of Alr. AH completed cell-based labeling experiments and growth curves. V.C.K. prepared and analyzed targeted metabolomic samples and characterized JW8. A.H. designed, executed and analyzed proteomic experiments. N.C.B. and M.S. contributed proteomics expertise and analyzed PLP binding sites. A.H. and S.A.S. wrote the manuscript.

Data availability
Supplementary information, chemical characterization and proteomic data analysis are available in the online version of the paper. Crystallographic data of alanine racemase structures have been deposited in the Protein Data Bank68 (www.rcsb.org) PDB codes: 6G56, 6G58, 6G59. The proteomic MS data (raw data and MaxQuant output tables for protein groups and peptides) have been deposited in the ProteomeXchange Consortium69 (http://proteomecentral.proteomexchange.org) via the PRIDE70 partner repository (data set identifier: PXD006483). Reprints and permissions information is available online at www.nature.com/reprints.

Competing interests
The authors declare no competing financial interests.

Europe PMC Funders Author Manuscripts

involved in essential cellular processes such as glucose, lipid and amino acid metabolism. To fulfill this range of tasks, PLP-DEs have acquired a large repertoire of chemical reactions, including transamination, α, β, γ-elimination, α, β, γ-replacement, racemization and decarboxylation. Despite this extraordinary diversity, PLP-DEs operate through some common mechanistic principles.4 In their resting state, PLP-DEs bind the PLP cofactor at active site lysine residues via a covalent imine bond termed the internal aldimine, which is displaced by an incoming substrate to form the external aldimine (Fig. 1a). PLP acts as an electrophilic catalyst which stabilizes negative charge at C_α by delocalization across an extended conjugated system as well as through electronic contributions of the protonated pyridine and Schiff base. Chemical specificity is fine-tuned by the interplay of PLP's intrinsic chemical properties and the surrounding protein matrix through stereoelectronic effects and hydrogen bonding. The size of the PLP-DE family is reflective of its diversity, catalyzing 238 distinct enzymatic functions5 and accounting for nearly 4% of all activities classified to date.6

Due to their widespread involvement in basic metabolic processes, PLP-DEs have been implicated in human disease and are recognized as important drug targets.1,7 PLP-DEs for which clinical drugs have been developed include alanine racemase (antibacterial agents), serine hydroxymethyltransferase (malaria, tumours), ornithine decarboxylase (African sleeping sickness), GABA aminotransferase (epilepsy), DOPA decarboxylase (Parkinson's), and branched-chain amino acid aminotransferase (GABA/glutamate equilibrium pathologies).1 However, modern therapies often suffer from severe side-effects as a consequence of off-target reactivity, a general challenge in designing PLP-DE inhibitors. Moreover, facing the threat of a post-antibiotic era, finding new and specific bacterial drug targets is becoming increasingly important. Since bacteria are estimated to share only a third of their PLP-DEs with humans,6 these enzymes may represent valuable antibacterial targets.

Gaining a global overview of PLP-DEs has been the subject of several bioinformatics-driven studies aimed at both identifying and functionally classifying PLP-DEs. While sequence similarity is notoriously low amongst PLP-DEs due to evolutionary disparity, structural similarity has led to their categorization into five distinct fold types.8 Methods capable of extracting structural conservation from genomic sequences have been useful for identifying PLP-DEs,5,6 though these strategies are restricted to known sequence-structure relationships. Further efforts have focused on identifying conserved active site features and surrounding regions using advanced database search tools,9–11 but these require structural information for the PLP-DEs. To date, there is no comprehensive method for profiling the cellular PLPome. It is thus estimated that many PLP-DEs remain unidentified and even more lack complete functional classification. While previous studies have visualized the PLPome by Western-blot (anti-pyridoxine antibodies), these methods are unable to identify or quantify distinct PLP-DEs.12 Moreover, proteomic studies are hampered by an inherent difficulty in identifying PLP-modified peptides due to their low intensity and stability during mass spectrometry measurement.13,14

Here we introduce a chemo-proteomic platform for the global identification and characterization of PLP-DEs in living cells. This platform uses functionalized pyridoxal (PL) cofactor mimics designed to be integrated into cellular PL uptake mechanisms and

metabolic processing to access the full complement of PLP-DEs in *Staphylococcus aureus*. Probe design and method development were guided by kinetic and structural studies using purified proteins, as well as cell-based metabolomic and proteomic experiments to ensure efficient probe processing. Implementation of a quantitative MS-based detection method revealed known as well as novel PLP-DE family members, facilitated a readout of relative cofactor binding abilities and enabled profiling of *in situ* inhibitor specificity.

Results

Design and synthesis of pyridoxal probes

Reporting on natural PLP binding events requires a functional, minimally-modified synthetic cofactor probe capable of labeling enzymes covalently. Previous investigations found that modifications at the 2-position of PLP, including either removal or limited expansion of the methyl group, could be tolerated by different PLP-DEs.15–17 Following the example of activity-based protein profiling,18 we designed PL-probes containing a small alkyne tag either directly attached to the pyridine ring (**PL1**) or with an ethylene spacer (**PL2**), and a 2'-azide analogue (**PL3**) to account for chemical preferences within protein binding sites (Fig. 1b). These probes were intended to make use of cellular PL-uptake mechanisms and metabolism to yield phosphorylated PLP derivatives capable of binding PLP-DEs (Fig. 1c). Our strategy capitalizes on the internal aldimine in order to anchor the probes to the enzymes irreversibly upon sodium borohydride ($NaBH_4$)-mediated reduction,13 circumventing the need for additional reactive groups. Subsequent bioorthogonal ligation of the alkyne tag to biotin-azide or *vice versa* allows gel- and MS-based detection of the full PLPome.

Syntheses of **PL1** and **PL3** were based on established chemical procedures, as detailed in Supplementary Schemes 1 and 2. While a 2'-alkynylated derivative of pyridoxine similar to **PL1** has previously been reported, it was not tested for viability as a cofactor.19 A structural isomer of **PL1** with inverse functionality at the 4' and 5' positions (**Ctrl**) that is electronically incapable of PLP catalysis was used as an inactive control probe to test for non-specific reactivity of the PL-scaffold. In the case of **PL2**, we devised an efficient new synthetic route using an alkylation strategy inspired by previous work on methylpyridine derivatives.20 **PL** was first protected as the cyclic monomethyl acetal21 followed by MOM-protection of the phenol to generate **1** (Fig. 1d). Deprotonation of the acidic 2-methyl position using LDA followed by reaction with propargyl bromide afforded the alkylated product **2**, which was deprotected under acidic conditions to yield **PL2** primarily in its hemiacetal form.22

In-depth biochemical characterization establishes efficient phosphorylation, binding, and catalysis of PL probes

Intracellular PLP homeostasis is regulated by pyridoxal kinase (PLK, Fig. 1a) which phosphorylates the B_6 vitamers PL, pyridoxine (PN) and pyridoxamine (PM) to suit the needs of the cell.23 Phosphorylation of PL is necessary for anchoring the cofactor to the internal aldimine site of PLP-DEs via hydrogen-bonding interactions.24 We first assessed our probes as substrates of *S. aureus* PLK using enzyme kinetics.25 Both **PL2** and **PL3** were

converted to phosphorylated products at levels comparable to PL (Fig. 2a), and formation of **PL2P** and **PL3P** was confirmed by MS/MS (Supplementary Fig. 1). Although significant overlap in the absorption spectra of NADH (340 nm) and **PL1** (325 nm, extended conjugation) precluded kinetic analysis, MS-based detection of **PL1P** confirmed phosphorylation by PLK (Supplementary Fig. 1). In contrast, no phosphorylation could be detected for the **Ctrl** probe.

Next, we examined the compatibility of the phosphorylated probes with alanine racemase (Alr) as a model PLP-DE since it is well-studied and universal to bacteria. Alr catalyzes the interconversion of L- and D-alanine, the latter of which is an essential component for peptidoglycan synthesis.26 Strep-tagged *S. aureus* Alr (Uniprot: P63479) was initially purified as the PLP-holoenzyme and transformed to the apoenzyme (Apo-Alr) by nucleophilic displacement of bound PLP using hydroxylamine. Reconstitution of Apo-Alr with phosphorylated probes yielded kinetically competent artificial holoenzymes with nearly identical efficiency compared to PLP-bound Alr (Fig. 2b). Probe binding and the degree of cofactor loading within the different holoenzymes were assessed spectrally by monitoring internal aldimine formation (410-430 nm,27 Fig. 2c) and by intact protein MS upon $NaBH_4$ reduction (Fig. 2d).

In order to understand the binding mode and accommodation of PLP-derivatives within the Alr active site, we determined the X-ray crystal structures of Alr bound to **PL1P** (PDB 6G58) and **PL2P** (PDB 6G59). Both cofactors bound the active site of Alr at the dimer interface and occupied the structurally equivalent position of the natural PLP-cofactor, linked to the highly conserved residue Lys39 as an internal aldimine (comparison with PDB 4A3Q,28 Fig. 2e and Supplementary Fig. 2). To accommodate the alkyne handle of the PLP-analogues, the sidechains of Lys131 and Arg138 realign slightly, though the active site geometry generally remains the same. This confirms the adequate space within the Alr aldimine binding pocket for accommodating the structural changes imparted to the synthetic cofactors without influencing catalytic activity. An overlay of additional known *S. aureus* PLP-DE crystal structures indicates that this extra space for probe binding is also a feature of other PLP-DEs (Supplementary Fig. 3).

Having established their authentic binding and functionality as cofactors, we next investigated whether the probes could label Alr *in vitro*. Incubation of Alr with **PL1P**, **PL2P** and **PL3P** probes, followed by reduction of the internal aldimine using $NaBH_4$ and conjugation to a rhodamine tag using copper-catalyzed azide-alkyne 1,3-dipolar cycloaddition (CuAAC, click chemistry), revealed specific labeling upon fluorescence SDS-PAGE (Fig. 2f).29–31 Unphosphorylated probes and the **Ctrl** probe (Supplementary Fig. 4) helped gauge nonspecific binding of the reactive aldehyde.

In-cell behaviour of PL probes reveals uptake and metabolism

The ability of our PL probes to function globally in native biological systems was evaluated using bacterial growth experiments. Microorganisms are capable of both *de novo* PLP biosynthesis (PLP-synthase complex, PdxS/PdxT) as well as PL salvage from the environment.32 In order to promote the uptake and use of our probes as PL surrogates, we used a *S. aureus* USA300 TnPdxS transposon mutant (Nebraska transposon mutant

library)33 that is incapable of *de novo* PLP biosynthesis but is able to salvage exogenous PL and convert it to PLP. Bacteria were incubated in PL-free medium supplemented with various concentrations of the probes and growth was measured after 24 h. In control experiments, less than 1 μM PL (Fig. 2g) supported maximum bacterial growth while absence of PL or incubation with **Ctrl** prohibited growth (OD_{600} < 0.1), thereby confirming the transposon phenotype. **PL1** and **PL3** afforded cellular growth in a concentration-dependent manner, though at higher concentrations than PL (approximately 25 μM), implying their effective integration into cellular metabolism (Fig. 2g). **PL2** did not support bacterial growth under the conditions tested, indicating that it cannot functionally substitute for all essential cellular PLP-processes. Nonetheless, when bacteria grown in rich medium were incubated with **PL2** over a 2-hour period, significant and concentration-dependent conversion to its phosphorylated **PL2P** form was revealed by MS (Fig. 2h). The observed metabolism of the probe suggested that adequate amounts of active probe could be generated under these conditions to allow for labeling experiments. Given the results of these cell-based studies, we proceeded with two proteomic labeling strategies tailored to the individual probe properties.

In situ labeling with PL2 provides direct, confident and rapid access to a large fraction of the PLPome

We first investigated the direct *in situ* labeling of *S. aureus* USA300 TnPdxS using **PL2**. Cultures grown in rich medium were subjected to different probe concentrations and incubation times, and, following cell lysis, reductive amination of the probe with cytosolic proteins and click chemistry to rhodamine azide, significant protein labeling was observed by fluorescence SDS-PAGE (Supplementary Fig. 5). Optimal labeling conditions (100 μM **PL2**, 2h incubation at 37°C) were established as a good balance between labeling strength and non-specific binding (Supplementary Fig. 5). With a viable labeling strategy in hand, we proceeded with in-depth proteomic evaluation of **PL2P**-binding in cells and conducted these experiments using two different probe concentrations (100 and 10 μM) and DMSO as a control. Conjugation of labeled proteins to a biotin-azide linker facilitated avidin-bead enrichment prior to trypsin digestion and LC-MS/MS analysis using label-free quantification (LFQ)34 (Fig. 3a). A large number of proteins were significantly enriched using 100 μM **PL2**, while fewer were detected at 10 μM (Supplementary Fig. 6). We observed a striking enrichment of proteins annotated to bind or utilize PLP (18 out of the 104 significant proteins) by gene ontology (GO-term: 0030170; PLP-binding) or EC classification at both concentrations (GO overrepresentation analysis for pyridoxal phosphate binding at 100 μM: enrichment factor 4.2, *p*-value $1.3e^{-10}$; at 10 μM: enrichment factor 16.0, *p*-value $3.3e^{-16}$). PLP-DEs of diverse functionality and fold type were identified, accounting for 40% of all PLP-DEs annotated in *S. aureus* USA300 so far (45 total) (Fig. 3c). By comparison, corresponding proteomic experiments performed with **PL1** and **PL3** (by Staudinger ligation) under the same conditions revealed fewer PLP-DE protein hits (Supplementary Fig. 7, 8, Supplementary Table 2,3). Nonetheless, the enriched proteins were distinct compared to **Ctrl**-treated cells, demonstrating that PLP-DE binding of our probes occurs specifically (Supplementary Fig. 7).

In order to distinguish PLP binding from background within this data set, we developed a confidence ranking that categorized all significantly enriched proteins into four classes based on their enrichment and LFQ-intensity profiles across these experiments (9 biological replicates total) (Fig. 3a). As PLP-DEs were reproducibly and concentration-dependently enriched, we reasoned that putative PLP binders should display similar profile behaviour. We therefore extracted the 10 most similar profiles (Perseus, Pearson correlation) of each known PLP-DE and grouped them together. Among these, we further defined high-confidence PLP-binding candidates as those proteins showing both similar profile behaviour and significant enrichment at the lower, and thus more selective, 10 μM probe concentration (18% of 104 significant proteins). These proteins were the same as the most significantly enriched proteins in the 100 μM experiment (approximate cut-off: fold-change ≥ 8; *p*-value ≤ 0.015). The remainder of the proteins from our profile search were assigned to a medium-confidence interval (28% of 104 significant proteins). Proteins whose intensity profiles resembled that of PLP-DEs less stringently ($11 \leq n \leq 20$ most similar profiles) were classified as low-confidence (19% of 104 significant proteins) and dissimilar profile behaviour was deemed background (35% of 104 significant proteins). These four confidence levels were mapped by colour onto the corresponding 100 μM volcano plot (Fig. 3b). In total, nearly half of the significantly enriched proteins were within the medium and high confidence intervals (Fig. 3c). Among them, we find known PLP-DEs, uncharacterized proteins and proteins annotated to have non-PLP-dependent functions. Since our data classifies the latter two categories as putative PLP-binders, these proteins represent a source for uncovering novel PLP-dependent roles within the cell. The complete list of significantly enriched proteins identified in this experiment can be found in Table 1 and Supplementary Table 1.

Having classified enriched proteins based on their similarity to PLP-DE profile behaviour, we next focused on the probe-binding properties of individual proteins. Proteomic experiments were performed using a larger range of probe concentrations in order to analyze the enrichment of proteins significantly identified in the above confidence plot (Fig. 3b). In plotting normalized LFQ-intensity profiles, we observed concentration-dependent probe binding of many proteins and were able to cluster their binding curve shapes into five groups of similar behaviour (Perseus, Pearson correlation, Fig. 3d) as illustrated by representative examples in Fig. 3a (bottom). Several proteins reached saturation at the applied probe concentrations (cluster 1) while, for others, the proportion of bound protein appeared to increase to differing degrees without reaching saturation (clusters 2-3). Proteins interacting with the probe non-specifically exhibited sporadic behaviour across the board (cluster 4-5). The majority of PLP-DEs fell into clusters 1 or 2, which depict the most defined binding curves over the range of concentrations tested and showed the largest proportion of high-confidence PLP-binding proteins (Fig. 3e). By applying this two-tiered filtering strategy – first defining PLP-DE confidence levels and secondly determining their binding behaviour – we were able to filter a large data set of enriched proteins obtained from our 2h-labeling protocol in order to select known PLP-DEs and uncharacterized proteins as candidates for further characterization.

Proteome mining of *S. aureus* cells supplemented with PL1 and PL3 during growth maximizes PLP-DE coverage

In a second proteomic approach, we capitalized on the ability of **PL1** and **PL3** to support *S. aureus* growth in order to increase probe integration into metabolic processes and thereby maximize PLP-DE labeling. Proteomic samples were prepared from *S. aureus* USA300 TnPdxS bacteria cultured directly in minimal medium supplemented with either **PL1**/**PL3** (25 μM for full growth) or PL (0.5 μM, control) (Fig. 4a). The commercially-available biotin-phosphine reagent35 (Supplementary Fig. 8) was used for the enrichment of **PL3**-labeled proteins via Staudinger ligation. MS analysis revealed significant and highly specific PLP-DE enrichment for probe-treated *versus* control samples. **PL1** labeling tallied at 16 PLP-DEs (enrichment factor 13.8, *p*-value $1.9e^{-17}$), which accounts for 36% of the currently annotated *S. aureus* PLPome (Fig. 4b, Supplementary Table 4) and thus shows comparable labeling efficiency to **PL2** (2h protocol). Using **PL3**, on the other hand, we covered over half of the *S. aureus* PLPome (26 proteins, 58%; enrichment factor 12.3, *p*-value $1.3e^{-28}$), representing the most complete PLP-DE labeling so far using our chemical proteomic strategy (Fig. 4c, Supplementary Table 5). Our results showed minimal background binding and several uncharacterized proteins among the significant population represent valuable leads for identifying new PLP-DEs. Importantly, this method facilitated access to 15 additional PLP-DEs not previously identified using **PL2** (Fig. 4d), thus increasing the total PLPome coverage to 73% (Fig. 4e).

UV-Vis, labeling and MS-based experiments validate PLP binding to known and uncharacterized PLP-DEs

To validate PLP-binding of proteins identified in our proteomics experiments, we first established a PLP-detection strategy with known PLP-DEs of different types, which were significantly enriched using our probes (**PL2** selection criteria: high, medium confidence; clusters 1, 2). These included two class I aminotransferases (AT1 and AT2; ID: A0A0H2XFY9 and A0A0H2XFA8), D-alanine aminotransferase (DAT; ID: A0A0H2XHU6), ornithine/lysine/arginine decarboxylase (ODC; ID: A0A0H2XII6) cysteine synthase (CS; ID: A0A0H2XFQ3) and a functionally uncharacterized PLP-DE predicted to be a PLP homeostasis regulator36,37 (HH8; ID: A0A0H2XHH8). We detected PLP binding to each of these proteins by UV-Vis (Fig. 5b, Supplementary Fig. 10) and observed characteristic spectral peaks indicative of their catalytic sequence and reaction type (Fig. 5a). 27,38 This allowed us to infer the aminotransferase activity of AT1, AT2 and DAT with different amino acids substrates by monitoring formation of PMP (330 nm), as well as CS activity by aminoacrylate (470 nm)27 formation with the substrate *O*-acetylserine (OAS) (Fig. 5b, Supplementary Fig. 10). Next, we corroborated PLP and **PL2P** binding to the selected PLP-DEs using intact protein MS. Incubation of the proteins with excess cofactor led to adduct formation (single-fold addition) upon $NaBH_4$ reduction (Fig. 5c, Supplementary Fig. 10, Supplementary Table 6). Control experiments using unphosphorylated cofactors (PL and **PL2**) proved the specificity of the interaction (Supplementary Table 6) and gel-based labeling experiments of the proteins with **PL2P** were in line with these observations (Fig. 5d). PLP binding was subsequently localized to exact lysine residues by digesting each of the six PLP-bound proteins with chymotrypsin and

analyzing resulting peptides by MS/MS (Fig. 5e,f). Identified PLP binding sites largely matched literature reports (Alr)28 and predicted sites (Interpro).39

We used the techniques established above to assess cofactor binding to four uncharacterized proteins: Q2FF14 (**PL1**, **PL2**: high-confidence, cluster 1), GP0 (ID: A0A0H2XGP0; **PL2**: medium-confidence, cluster 2), IC2 (ID: A0A0H2XIC2; **PL3**) and IU9 (ID: A0A0H2XIU9; **PL3**). Each protein appeared to bind PLP and the probes based on UV-Vis, MS and gel-based labeling experiments (Fig. 5b, c, d, f). While MS analysis confirmed PLP binding to IC2 and IU9, detection of **PL3P** binding, though clearly visible by fluorescent SDS-gel analysis (Fig. 5d), was difficult probably due to impaired ionization or stability. A few proteins with alternative, non-PLP-related functions significantly enriched in proteomic experiments were also examined (Supplementary Fig. 12). These showed either nonspecific or minimal binding, implying a weak or transient interaction with the cofactor, or unsuitable experimental conditions for detecting the interaction.

Our next goal was to apply our method to annotate unclear or unknown protein functions. We therefore exemplarily selected the putative PLP-dependent acyltransferase JW8 (ID: A0A0H2XJW8; identified by all probes) in order to assign its catalytic role. A spectrophotometric acetylation assay40 with acetyl-CoA was used to screen a variety of amino acid substrates for JW8, and glycine was identified as the preferred substrate (Supplementary Fig. 13). The requirement of the PLP cofactor for catalyzing this reaction was confirmed using inactivated JW8 ($NaBH_4$ reduction of the internal aldimine) as a negative control. We can therefore ascribe JW8 the function of a glycine acetyltransferase (2-amino-3-ketobutyrate CoA ligase CoA ligase), which constitutes a known PLP-dependent reaction.41 Next, we tackled the functional annotation of the uncharacterized protein IU9. The gene encoding IU9 (SAUSA300_0700) is located in an operon together with *para*-aminobenzoic acid (PABA) synthase components PabA (glutamine amidotransferase) and PabB (aminodeoxychorismate synthase), which catalyze the amination of chorismate using NH_3 to yield aminodeoxychorismate (Fig. 5g). We thus reasoned that IU9 may also have a role in PABA biosynthesis or a related process, which is an important precursor for folate production. In fact, a third enzyme involved in PABA biosynthesis, called PabC (aminodeoxychorismate lyase), has previously been recognized to catalyze PABA formation from aminodeoxychorismate in a PLP-dependent manner, generating pyruvate as a byproduct.42 We investigated the possibility of IU9 to catalyze this reaction using a coupled assay42 which detects pyruvate production upon incubation of chorismate with purified PabB (recombinantly expressed from *Escherichia coli*) and IU9 (Fig. 5h). Our results show IU9-dependent formation of PABA and the product identity was confirmed by MS comparison to a synthetic standard (Fig. 5i). We conclude that the uncharacterized protein IU9 represents an aminodeoxychorismate lyase for PABA production in *S. aureus*.

Proteome-wide analysis of structural constraints within PLP-binding sites

As a result of evolutionary and chemical necessity, PLP-DEs can accommodate diverse structures in their active sites and tolerate modifications of the PLP scaffold to varying extents. In order to profile structural constraints within PLP-binding sites on a global level, we synthesized two additional PL probes bearing increased steric bulk at the 2-position,

Europe PMC Funders Author Manuscripts

including an extended alkyl chain (**PL4**) and an aromatic linker (**PL5**) (Fig. 6a, Supplementary Scheme 3). Despite reduced enzymatic turnover by PLK compared to **PL2**, likely due to unfavourable interactions within the PLK active site (Supplementary Fig. 3), formation of the phosphorylated probe products could nonetheless be detected by MS upon incubation with PLK (Supplementary Fig. 15). Significant gel-based labeling of *S. aureus* USA300 TnPdxS with **PL4** and **PL5** following our 2h *in situ* labeling protocol (Fig. 6b) prompted us to evaluate these probes using MS-based proteomics. Comparison of the relative LFQ-intensities of PLP-DEs enriched using **PL2**, **PL4** and **PL5** revealed trends in structural tolerance among the enzymes (Fig. 6c). Generally, PLP-DEs were identified at successively lower intensities as structural bulk at the 2-methyl position increased and nearly half of the proteins were only strongly enriched using **PL2**, including the uncharacterized protein Q2FF14. Significantly more background labeling was also observed. Interestingly, proteins such as cysteine synthase (A0A0H2XFQ3), the class-I aminotransferase (A0A0H2XFY9), cystathionine gamma-synthase (A0A0H2XFF8), and the uncharacterized putative PLP-homeostasis protein (A0A0H2XHH8) all tolerated the extended chain of **PL4** well and were identified with intensities in the range of **PL2**-based labeling. Similarly, alanine racemase (Q2FF55), which was proven to accommodate structural alterations of the cofactor, was also significantly enriched using **PL4**. Other proteins, including threonine synthase (A0A0H2XH24), threonine deaminase (Q2FH01) and the uncharacterized protein A0A0H2XGP0 preferred the aromatic bulk of **PL5**. This study acts as a proof-of-concept for how PLP-derivatives can be applied to actively probe space within PLP binding sites on a proteome-wide level and help define structure-activity and structure-selectivity relationships across a panel of PLP-DEs.

Screening of D-cycloserine activity using PL2 reveals new off-targets

Inhibitors of PLP-DEs often lack specificity due to active site similarities among enzyme family members, which limits their use. D-cycloserine (DCS), for example, is an antibiotic known to inhibit several PLP-DEs, including racemases,26 transaminases43 and decarboxylases,44 which shows severe toxic side effects.45,46 DCS targets bacterial peptidoglycan synthesis by reversibly inhibiting Alr, D-ala-D-ala ligase (Ddl),26,47 and DAT,43 forming a stable aromatic PLP derivative within the enzyme pockets (Fig. 6d).48,49 In line with previous literature reports,50,51 we observed concentration-dependent inhibition of DCS on Alr activity *in vitro* (Supplementary Fig. 17) and a minimum inhibitory concentration (MIC) of 0.5 mM in *S. aureus*. In order to screen for other PLP-DEs inhibited by DCS, we designed a competitive proteomic experiment in which *S. aureus* USA300 TnPdxS was incubated with DCS for 30 min prior to conducting our 2h labeling protocol with **PL2**. Upon plotting the difference in non-treated versus DCS-treated samples (Fig. 6e), we identified a handful of enzymes significantly influenced by DCS in a concentration-dependent manner (Fig. 6f). Among these was the known target DAT, as well as two previously undescribed PLP-DE targets, ODC and diaminopimelate decarboxylase (DAPDC). Interestingly, Alr was not significantly affected by DCS under these conditions. While this is in disagreement with several *in vitro* studies,51,52 recent metabolomics experiments in mycobacteria also suggest that Alr is weakly inhibited by DCS in a cellular context, while Ddl is the primary lethal target.53,54 This observation could be explained by the substrate promiscuity often displayed by PLP-DEs *in vitro*.55,56 Furthermore, we were

surprised to identify Ddl in our experiment, which, despite being a known target of DCS and under PLP-based transcriptional regulation,57 is not known to interact with PLP. Our proteomic data (Fig. 3b, Table 1) suggests that it may interact with **PL2P**, as we find it significantly enriched (medium-confidence).

Discussion

We describe the development of a novel toolset for profiling the PLP-dependent proteome which is easily accessible, compatible with biological systems and adaptable to suit diverse chemical biology needs. We provide a means for the modular derivatization of PL at the 2'-position, where modifications were well tolerated by a variety of proteins. Examples include PLK, the first critical cellular hurdle for generating active probes *in situ*, as well as Alr, a PLP-DE capable of accommodating different PLP structures without influencing its catalytic activity. Modulation with different substituents at this position also showed some ability to target different parts of the PLPome. We show for the first time that minimally modified synthetic vitamers (**PL1** and **PL3**) can globally substitute for essential cellular PLP processes in order to support bacterial growth. Labeling under these conditions accesses the highest number of PLP-DEs, likely due to effective integration into biological systems. Although the ethylene linker of **PL2** may be too large to be functionally tolerated by all essential PLP-DEs, it can nonetheless bind to a large portion of the *S. aureus* PLPome in an effective 2h-labeling strategy with stringent data filtering. Crystallographic snapshots showed formation of an internal aldimine linkage between our probes and Alr, which acts as a suitable handle for attaching chemical tags to PLP-DEs via reductive amination while avoiding the use of cumbersome and inherently non-specific photocrosslinking moieties58 or electrophilic traps. We find the reactive PLP aldehyde to bind active site lysines specifically, as evidenced by minimal background labeling and negative binding controls (**Ctrl** and unphosphorylated probes) in our analytical and proteomic experiments. Our studies confirm the authenticity and specificity of probe binding in the complex environment of the living cell and provide a blueprint for future probe and experimental design.

We introduce two effective labeling strategies capable of a) extending labeling coverage by metabolic incorporation of synthetic cofactor probes throughout bacterial growth, and b) rapid labeling for *in situ* applications with simplified experimental requirements. This allowed us to access 73% of the current *S. aureus* PLPome and to identify many more putative PLP binding events. Our findings were strengthened by extended MS-based analyses of LFQ-intensity profiles across multiple probe concentrations, which enabled us to categorize proteins into different confidence classes and to cluster similar probe binding-behaviour among proteins. Our method pre-selects proteins of unknown function as PLP-dependent, and thereby enables customized investigations to unravel their function. We illustrate its utility in assigning glycine acetyltransferase activity to the putative PLP-dependent acyltransferase JW8. Moreover, our approach enabled the high-confidence annotation of uncharacterized proteins Q2FF14, GP0 and IC2 as potentially novel PLP-DEs as well as identifying IU9 as an aminodeoxychorismate lyase in *S. aureus*. We anticipate that our probe will provide a resource for unraveling new PLP roles or yet undiscovered interactions in a cellular context.

Europe PMC Funders Author Manuscripts

Our strategy addresses shortcomings in PLP-based drug development by screening for off-target reactivity of PLP-DE inhibitors. We here focused on the anti-tuberculosis drug DCS and identified two decarboxylases as potential novel targets using competitive proteomic experiments. Surprisingly, we find that Alr is not significantly affected by DCS treatment in a cellular context despite its proven inhibition *in vitro*. Learning more about the off-target mechanisms of PLP-DE inhibitors allows us to pinpoint ways to improve current therapies and our method also provides a means for identifying new PLP-DEs as potential drug targets. Furthermore, *in situ* SAR-profiling across a panel of probes can serve as a starting point for understanding active site geometries of different PLP-DEs and their selectivity.

A current limitation of our PLP-DE detection strategy is the need to force probe uptake using a bacterial transposon mutant devoid of *de novo* PLP biosynthesis. However, this is allayed by the availability of corresponding transposon mutants in a host of bacterial systems as well as the fact that eukaryotes lack PLP biosynthetic machinery and rely solely on PL salvage. In addition, the influence of structural modifications of PL limits our access to enzymes with restricted binding sites. As evidenced by growth experiments, our probes appear to substitute for PLP incompletely, which prevents us from reporting on the full complement of PLP-DEs.

Profiling the PLPome lays important groundwork for studying diverse topics of interest within the field, such as evolutionary relationships of PLP-DEs, alternative functions of PLP and the comparison of different organisms, cell types or cell states. The ability to simultaneously monitor several PLP-DEs in a natural context and to identify novel family members or functions without prior information has the potential to fill major gaps in our knowledge of PLP-DEs. A key challenge in the field remains the full functional characterization of novel PLP-DEs upon their identification, which necessitates combined biochemical, structural and bioinformatics approaches. While previous flowcharts for characterizing unknown PLP-DEs serve as a useful starting point,11 the picture remains largely incomplete and requires expansion through significant experimental work to additionally address individual cases.

Our methodology provides the first detailed proteomic perspective on the family of PLP-DEs and is concurrent with other recent endeavours in profiling post-translational modifications and cofactor-dependent families.59–64 Efforts to effectively mine proteomes for important cellular players not only increase our understanding of different protein families, but are fundamental to the development of biomarkers and therapeutics. These studies therefore provide efficient measures for tackling the wealth of uncharacterized proteins still awaiting exploration.

Methods

See Supporting Information for detailed methods and protocols.

Sample preparation and MS-based proteomic analysis

(**2h *in situ* protocol**): A stationary phase culture of *S. aureus* USA300 TnPdxS (Nebraska transposon mutant library)33 grown in B-medium was exchanged into chemically-defined

(PL-free) medium (CDM) containing 5 μg/ml Erythromycin and adjusted to OD_{600} = 40. For each sample, 1 ml of this suspension (≈ 1 mg protein) was incubated with 10 μl probe or DMSO (100× stock in DMSO) for 2 h at 37°C and bacteria were washed with PBS prior to cell lysis. (Chemical supplementation method): Overnight cultures of *S. aureus* USA300 TnPdxS grown in B-medium were washed in CDM-Erm and used to inoculate cultures (to OD_{600} = 0.1) in CDM-Erm (100 ml) supplemented with 25 μM probe (25 μl of 100 mM stock in DMSO) or 0.5 μM PL (25 μl of 2 mM stock in DMSO) in baffled flasks. Bacteria were grown to stationary phase (30 h at 37°C), harvested, washed with PBS and adjusted to 1 ml OD_{600} = 60 (≈ 2 mg protein) prior to cell lysis. For the remainder of the protocol, all samples were handled the same. Cells were lysed mechanically (Precellys Lysing Kit and Homogenizer) and clarified cytosolic fractions were reduced with 20 mM $NaBH_4$ (prepared fresh in 0.1 M NaOH) for 30 min at rt. Following protein precipitation, samples were solubilized (PBS containing 0.4% SDS) and conjugated by CuAAC to a tri-functional rhodamine-biotin-azide.65 **PL3**-labeled samples were instead conjugated to EZ-Link™ Phosphine-PEG_3-Biotin (Sigma Aldrich) via Staudinger ligation (0.2 mM per 1 ml sample, 2 mg protein, 4 h at 37°C, then 20 h at 25°C). Upon avidin-bead enrichment, samples were reduced with 5 mM TCEP (1 h at 37°C), alkylated using 10 mM IAA (30 min at 25°C) and quenched with 10 mM DTT (30 min at 25°C) on-bead. Proteins were pre-digested using LysC (2 h at 25°C) and then digested with trypsin (16 h at 37°C). Samples were desalted using SepPak C18 cartridges (50 mg, Waters) prior to MS-measurement. All samples were prepared in three biological replicates from individual starting cultures and were processed in parallel. LC-MS/MS analysis was performed with an Ultimate3000 Nano-HPLC system (Thermo Fisher Scientific) coupled to an Orbitrap Fusion instrument (Thermo Fisher Scientific). Data were acquired using Xcalibur software version 3.0sp2 (Thermo Fisher Scientific). MS raw files were analyzed with MaxQuant66 software (version 1.5.3.8). MS/MS-based peptide identification was carried out using the Andromeda67 search engine with the *S. aureus* USA300 UniProtKB database (May 2016, 2607 accessions). Statistical analysis was performed in Perseus (version 1.5.5.3). Data were filtered to retain only those proteins with > 2 MS/MS counts and quantified in at least 2 out of 3 replicates (alternatively, 5/6 or 8/9 replicates). Missing values were imputed on the basis of a normal distribution and volcano plots were generated by performing a two-sample t-test with permutation-based statistics (FDR 0.05, s0 = 1). See supporting information for a detailed description of the proteomic workflow.

Supplementary Material

Refer to Web version on PubMed Central for supplementary material.

Acknowledgements

This project received funding from the European Research Council (ERC) and the European Union's Horizon 2020 research and innovation programme (grant agreement No 725085, CHEMMINE, ERC consolidator grant). Further financial support includes doctoral scholarships to A.H. from the Deutscher Akademischer Austausch Dienst (DAAD) and to M.S. from the Studienstiftung des Deutschen Volkes. We thank the Network on Antimicrobial Resistance in *Staphylococcus aureus* (NARSA) for the supply of the Nebraska Transposon Mutant Library (NTML). We thank Mona Wolff and Katja Bäuml for technical assistance. We also thank the Swiss Light Source (SLS) and European Synchrotron Radiation Facility (ESRF) for beamtime and the staff of beamlines PX I (SLS), ID23-2 and ID29 (ESRF) for setup and data collection. We gratefully acknowledge M. H. Wright and B. M. Williams for critical proofreading of the manuscript.

References

1. Amadasi A, et al. Pyridoxal 5'-phosphate enzymes as targets for therapeutic agents. Curr Med Chem. 2007; 14:1291–1324. [PubMed: 17504214]
2. Di Salvo ML, Budisa N, Contestabile R. Beilstein Bozen Symposium on Molecular Engineering and Control. Beilstein-Institut; Prien (Chiemsee), Germany: 2013. 27–66.
3. Eliot AC, Kirsch JF. Pyridoxal phosphate enzymes: mechanistic, structural, and evolutionary considerations. Annu Rev Biochem. 2004; 73:383–415. [PubMed: 15189147]
4. Toney MD. Reaction specificity in pyridoxal phosphate enzymes. Arch Biochem Biophys. 2005; 433:279–287. [PubMed: 15581583]
5. Percudani R, Peracchi A. The B6 database: a tool for the description and classification of vitamin B6-dependent enzymatic activities and of the corresponding protein families. BMC Bioinformatics. 2009; 10:273. [PubMed: 19723314]
6. Percudani R, Peracchi A. A genomic overview of pyridoxal-phosphate-dependent enzymes. EMBO Rep. 2003; 4:850–854. [PubMed: 12949584]
7. Kappes B, Tews I, Binter A, Macheroux P. PLP-dependent enzymes as potential drug targets for protozoan diseases. Biochim Biophys Acta. 2011; 1814:1567–1576. [PubMed: 21884827]
8. Mehta PK, Christen P. The molecular evolution of pyridoxal-5'-phosphate-dependent enzymes. Adv Enzymol Relat Areas Mol Biol. 2000; 74:129–184. [PubMed: 10800595]
9. Catazaro J, Caprez A, Guru A, Swanson D, Powers R. Functional evolution of PLP-dependent enzymes based on active-site structural similarities. Proteins. 2014; 82:2597–2608. [PubMed: 24920327]
10. Denessiouk KA, Denesyuk AI, Lehtonen JV, Korpela T, Johnson MS. Common structural elements in the architecture of the cofactor-binding domains in unrelated families of pyridoxal phosphate-dependent enzymes. Proteins. 1999; 35:250–261. [PubMed: 10223296]
11. Fleischman NM, et al. Molecular characterization of novel pyridoxal-5'-phosphate-dependent enzymes from the human microbiome. Protein Sci. 2014; 23:1060–1076. [PubMed: 24888348]
12. Whittaker MM, Penmatsa A, Whittaker JW. The Mtm1p carrier and pyridoxal 5'-phosphate cofactor trafficking in yeast mitochondria. Arch Biochem Biophys. 2015; 568:64–70. [PubMed: 25637770]
13. Simon ES, Allison J. Determination of pyridoxal-5'-phosphate (PLP)-bonding sites in proteins: a peptide mass fingerprinting approach based on diagnostic tandem mass spectral features of PLP-modified peptides. Rapid Commun Mass Spectrom. 2009; 23:3401–3408. [PubMed: 19810014]
14. Wu Y, Chen J, Liu Z, Wang F. Identification of pyridoxal phosphate modified proteins using mass spectrometry. Rapid Commun Mass Spectrom. 2017
15. Schnackerz KD, Cook PF. Resolution of pyridoxal 5'-phosphate from O-acetylserine sulfhydrylase from Salmonella typhimurium and reconstitution of apoenzyme with cofactor and cofactor analogues as a probe of the cofactor binding site. Arch Biochem Biophys. 1995; 324:71–77. [PubMed: 7503562]
16. Morino Y, Snell EE. Coenzyme activity of homologues of pyridoxal phosphate. Biochemistry. 1967; 57:1692–1699.
17. Mechanik ML, Torchinsky YM, Florentiev VL, Karpeisky MY. Interaction of the apoenzyme of L-glutamate decarboxylase with pyridoxal phosphate analogues. FEBS Lett. 1971; 13:177–180. [PubMed: 11945661]
18. Cravatt BF, Wright AT, Kozarich JW. Activity-based protein profiling: from enzyme chemistry to proteomic chemistry. Annu Rev Biochem. 2008; 77:383–414. [PubMed: 18366325]
19. Korytnyk W, Srivastava SC, Angelino N, Potti PG, Paul B. A general method for modifying the 2-methyl group of pyridoxol. Synthesis and biological activity of 2-vinyl- and 2-ethynylpyridoxols and related compounds. J Med Chem. 1973; 16:1096–1101. [PubMed: 4749469]
20. Kaiser EM, et al. Regiointegrity of carbanions derived by selective metalations of dimethylpyridines and -quinolines. J Organomet Chem. 1981; 213:405–417.
21. Kim Y-C, Jacobson KA. Versatile synthesis of 6-alkyl and aryl substituted pyridoxal derivatives. Synthesis. 2000; 1:119–122.

22. Korytnyk W, Ahrens H. 5-homopyridoxals, 5-thiopyridoxal, and related compounds. Synthesis, tautomerism, and biological properties. J Med Chem. 1971; 14:947–952. [PubMed: 4398921]
23. di Salvo ML, Contestabile R, Safo MK. Vitamin B(6) salvage enzymes: mechanism, structure and regulation. Biochim Biophys Acta. 2011; 1814:1597–1608. [PubMed: 21182989]
24. Denesyuk AI, Denessiouk KA, Korpela T, Johnson MS. Functional attributes of the phosphate group binding cup of pyridoxal phosphate-dependent enzymes. J Mol Biol. 2002; 316:155–172. [PubMed: 11829510]
25. Nodwell MB, Koch MF, Alte F, Schneider S, Sieber SA. A subfamily of bacterial ribokinases utilizes a hemithioacetal for pyridoxal phosphate salvage. J Am Chem Soc. 2014; 136:4992–4999. [PubMed: 24601602]
26. Strominger JL, Ito I, Threnn RH. Competitive inhibition of enzymatic reactions by oxamycin. J Am Chem Soc. 1960; 82:998–999.
27. Griswold WR, Toney MD. Role of the pyridine nitrogen in pyridoxal 5'-phosphate catalysis: activity of three classes of PLP enzymes reconstituted with deazapyridoxal 5'-phosphate. J Am Chem Soc. 2011; 133:14823–14830. [PubMed: 21827189]
28. Scaletti ER, Luckner SR, Krause KL. Structural features and kinetic characterization of alanine racemase from Staphylococcus aureus (Mu50). Acta Crystallogr D Biol Crystallogr. 2012; 68:82–92. [PubMed: 22194336]
29. Rostovtsev VV, Green LG, Fokin VV, Sharpless KB. A stepwise huisgen cycloaddition process: copper(I)-catalyzed regioselective "ligation" of azides and terminal alkynes. Angew Chem Int Ed Engl. 2002; 41:2596–2599. [PubMed: 12203546]
30. Speers AE, Cravatt BF. Profiling enzyme activities in vivo using click chemistry methods. Chem Biol. 2004; 11:535–546. [PubMed: 15123248]
31. Tornoe CW, Christensen C, Meldal M. Peptidotriazoles on solid phase: [1,2,3]-triazoles by regiospecific copper(i)-catalyzed 1,3-dipolar cycloadditions of terminal alkynes to azides. J Org Chem. 2002; 67:3057–3064. [PubMed: 11975567]
32. Mukherjee T, Hanes J, Tews I, Ealick SE, Begley TP. Pyridoxal phosphate: biosynthesis and catabolism. Biochim Biophys Acta. 2011; 1814:1585–1596. [PubMed: 21767669]
33. Fey PD, et al. A genetic resource for rapid and comprehensive phenotype screening of nonessential Staphylococcus aureus genes. MBio. 2013; 4 e00537-00512. doi: 10.1128/mBio.00537-12
34. Cox J, et al. Accurate proteome-wide label-free quantification by delayed normalization and maximal peptide ratio extraction, termed MaxLFQ. Mol Cell Proteomics. 2014; 13:2513–2526. [PubMed: 24942700]
35. Saxon E, Bertozzi CR. Cell surface engineering by a modified Staudinger reaction. Science. 2000; 287:2007–2010. [PubMed: 10720325]
36. Ito T, et al. Conserved pyridoxal protein that regulates Ile and Val metabolism. J Bacteriol. 2013; 195:5439–5449. [PubMed: 24097949]
37. Prunetti L, et al. Evidence That COG0325 Proteins are involved in PLP Homeostasis. Microbiology. 2016; doi: 10.1099/mic.0.000255
38. Mozzarelli A, Bettati S. Exploring the pyridoxal 5'-phosphate-dependent enzymes. Chem Rec. 2006; 6:275–287. [PubMed: 17109392]
39. Finn RD, et al. InterPro in 2017-beyond protein family and domain annotations. Nucleic Acids Res. 2017; 45:D190–D199. [PubMed: 27899635]
40. Kuhn ML, Majorek KA, Minor W, Anderson WF. Broad-substrate screen as a tool to identify substrates for bacterial Gcn5-related N-acetyltransferases with unknown substrate specificity. Protein Sci. 2013; 22:222–230. [PubMed: 23184347]
41. Mukherjee JJ, Dekker EE. Purification, properties, and N-terminal amino acid sequence of homogeneous Escherichia coli 2-amino-3-ketobutyrate CoA ligase, a pyridoxal phosphate-dependent enzyme. J Biol Chem. 1987; 262:14441–14447. [PubMed: 3117785]
42. Ye QZ, Liu J, Walsh CT. p-Aminobenzoate synthesis in Escherichia coli: purification and characterization of PabB as aminodeoxychorismate synthase and enzyme X as aminodeoxychorismate lyase. Proc Natl Acad Sci USA. 1990; 87:9391–9395. [PubMed: 2251281]

Europe PMC Funders Author Manuscripts

43. Soper TS, Manning JM. Different modes of action of inhibitors of bacterial D-amino acid transaminase. A target enzyme for the design of new antibacterial agents. J Biol Chem. 1981; 256:4263–4268. [PubMed: 7217082]
44. Malashkevich VN, Strop P, Keller JW, Jansonius JN, Toney MD. Crystal structures of dialkylglycine decarboxylase inhibitor complexes. J Mol Biol. 1999; 294:193–200. [PubMed: 10556038]
45. Yew WW, Wong CF, Wong PC, Lee J, Chau CH. Adverse neurological reactions in patients with multidrug-resistant pulmonary tuberculosis after coadministration of cycloserine and ofloxacin. Clin Infect Dis. 1993; 17:288–289. [PubMed: 8399888]
46. Caminero JA, Sotgiu G, Zumla A, Migliori GB. Best drug treatment for multidrug-resistant and extensively drug-resistant tuberculosis. Lancet Infect Dis. 2010; 10:621–629. [PubMed: 20797644]
47. Neuhaus FC. Selective inhibition of enzymes utilizing alanine in the biosynthesis of peptidoglycan. Antimicrob Agents Chemother (Bethesda). 1967; 7:304–313. [PubMed: 5596153]
48. Peisach D, Chipman DM, Van Ophem PW, Manning JM, Ringe D. D-cycloserine inactivation of D-amino acid aminotransferase leads to a stable noncovalent protein complex with an aromatic cycloserine-PLP derivative. J Am Chem Soc. 1998; 120:2268–2274.
49. Fenn TD, Stamper GF, Morollo AA, Ringe D. A side reaction of alanine racemase: transamination of cycloserine. Biochemistry. 2003; 42:5775–5783. [PubMed: 12741835]
50. Sieradzki K, Tomasz A. Suppression of beta-lactam antibiotic resistance in a methicillin-resistant Staphylococcus aureus through synergic action of early cell wall inhibitors and some other antibiotics. J Antimicrob Chemother. 1997; 39:47–51. [PubMed: 9511062]
51. Roze U, Strominger JL. Alanine racemase from Staphylococcus aureus: conformation of its substrates and its inhibitor, D-cycloserine. Mol Pharm. 1966; 2:92–94.
52. Lambert MP, Neuhaus FC. Mechanism of D-cycloserine action: alanine racemase from Escherichia coli W. J Bacteriol. 1972; 110:978–987. [PubMed: 4555420]
53. Prosser GA, de Carvalho LP. Metabolomics Reveal d-Alanine:d-Alanine Ligase As the Target of d-Cycloserine in Mycobacterium tuberculosis. ACS Med Chem Lett. 2013; 4:1233–1237. [PubMed: 24478820]
54. Halouska S, et al. Metabolomics analysis identifies d-Alanine-d-Alanine ligase as the primary lethal target of d-Cycloserine in mycobacteria. J Proteome Res. 2014; 13:1065–1076. [PubMed: 24303782]
55. Contestabile R, et al. l-Threonine aldolase, serine hydroxymethyltransferase and fungal alanine racemase. A subgroup of strictly related enzymes specialized for different functions. Eur J Biochem. 2001; 268:6508–6525. [PubMed: 11737206]
56. di Salvo ML, et al. Alanine racemase from Tolypocladium inflatum: a key PLP-dependent enzyme in cyclosporin biosynthesis and a model of catalytic promiscuity. Arch Biochem Biophys. 2013; 529:55–65. [PubMed: 23219598]
57. Takenaka T, Ito T, Miyahara I, Hemmi H, Yoshimura T. A new member of MocR/GabR-type PLP-binding regulator of D-alanyl-D-alanine ligase in Brevibacillus brevis. FEBS J. 2015; 282:4201–4217. [PubMed: 26279274]
58. Kleiner P, Heydenreuter W, Stahl M, Korotkov VS, Sieber SA. A Whole Proteome Inventory of Background Photocrosslinker Binding. Angew Chem Int Ed Engl. 2017; 56:1396–1401. [PubMed: 27981680]
59. Anderson LN, et al. Live Cell Discovery of Microbial Vitamin Transport and Enzyme-Cofactor Interactions. ACS Chem Biol. 2016; 11:345–354. [PubMed: 26669591]
60. Broncel M, Serwa RA, Bunney TD, Katan M, Tate EW. Global Profiling of Huntingtin-associated protein E (HYPE)-Mediated AMPylation through a Chemical Proteomic Approach. Mol Cell Proteomics. 2016; 15:715–725. [PubMed: 26604261]
61. Grammel M, Hang HC. Chemical reporters for biological discovery. Nat Chem Biol. 2013; 9:475–484. [PubMed: 23868317]
62. Romine MF, et al. Elucidation of roles for vitamin B12 in regulation of folate, ubiquinone, and methionine metabolism. Proc Natl Acad Sci USA. 2017; 114:E1205–E1214. [PubMed: 28137868]
63. Westcott NP, Fernandez JP, Molina H, Hang HC. Chemical proteomics reveals ADP-ribosylation of small GTPases during oxidative stress. Nat Chem Biol. 2017; 13:302–308. [PubMed: 28092360]

64. Wright MH, et al. Validation of N-myristoyltransferase as an antimalarial drug target using an integrated chemical biology approach. Nat Chem. 2014; 6:112–121. [PubMed: 24451586]
65. Eirich J, et al. Pretubulysin derived probes as novel tools for monitoring the microtubule network via activity-based protein profiling and fluorescence microscopy. Mol Biosyst. 2012; 8:2067–2075. [PubMed: 22722320]
66. Tyanova S, Temu T, Cox J. The MaxQuant computational platform for mass spectrometry-based shotgun proteomics. Nat Protoc. 2016; 11:2301–2319. [PubMed: 27809316]
67. Cox J, et al. Andromeda: a peptide search engine integrated into the MaxQuant environment. J Proteome Res. 2011; 10:1794–1805. [PubMed: 21254760]
68. Berman HM, et al. The Protein Data Bank. Nucleic Acids Research. 2000; 28:235–242. [PubMed: 10592235]
69. Vizcaino JA, et al. ProteomeXchange provides globally coordinated proteomics data submission and dissemination. Nat Biotechnol. 2014; 32:223–226. [PubMed: 24727771]
70. Vizcaino JA, et al. 2016 update of the PRIDE database and its related tools. Nucleic Acids Res. 2016; 44:11033. [PubMed: 27683222]

Europe PMC Funders Author Manuscripts

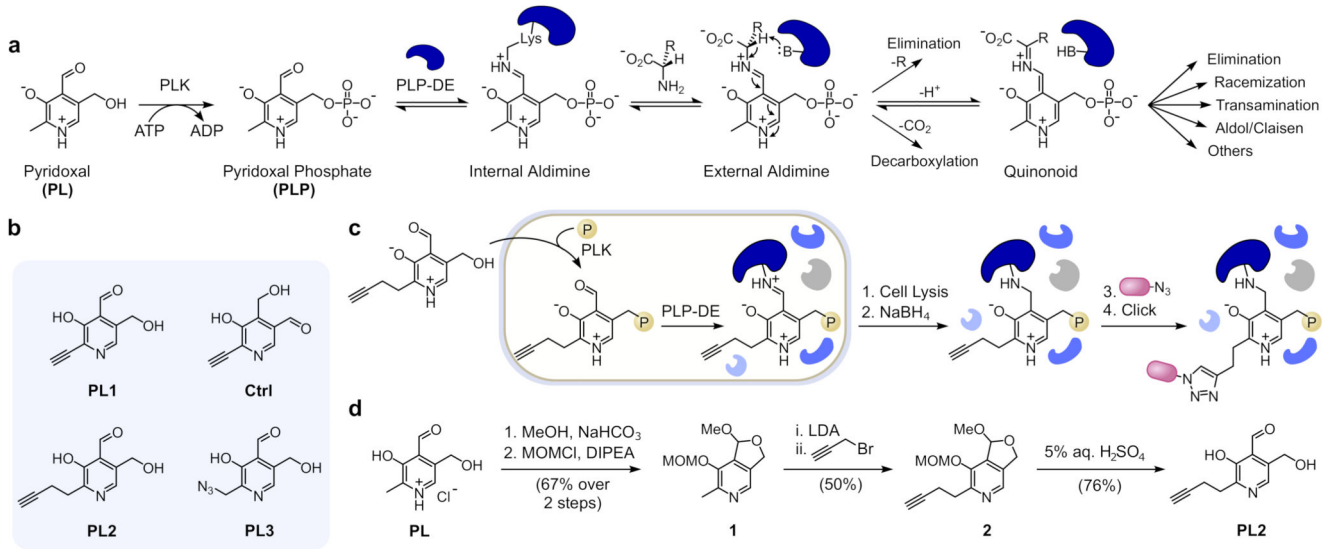

Figure 1. Design and synthesis of PL-probes.

(**a**) PL is phosphorylated by cellular PLK and PLP then binds PLP-DEs at active site lysine residues via an internal aldimine. Transamination with substrate amines forms the external aldimine which enables diverse chemical transformations via select quinonoid formation. (**b**) The chemical structures of PL-probes **PL1**, **PL2**, **PL3** and the **Ctrl**. (**c**) PLPome detection strategy. PL-probes are taken up by *S. aureus* cells, phosphorylated, and incorporated into PLP-DEs. Upon cell lysis, $NaBH_4$ reduction of the imine bond and click chemistry with fluorescent or enrichment tags permits proteomic identification of labeled PLP-DEs. (**d**) Synthesis of **PL2** by alkylation of the 2-methyl position of PL. MOM = methoxymethyl, DIPEA = *N,N*-Diisopropylethylamine, LDA = lithium diisopropylamine.

Europe PMC Funders Author Manuscripts

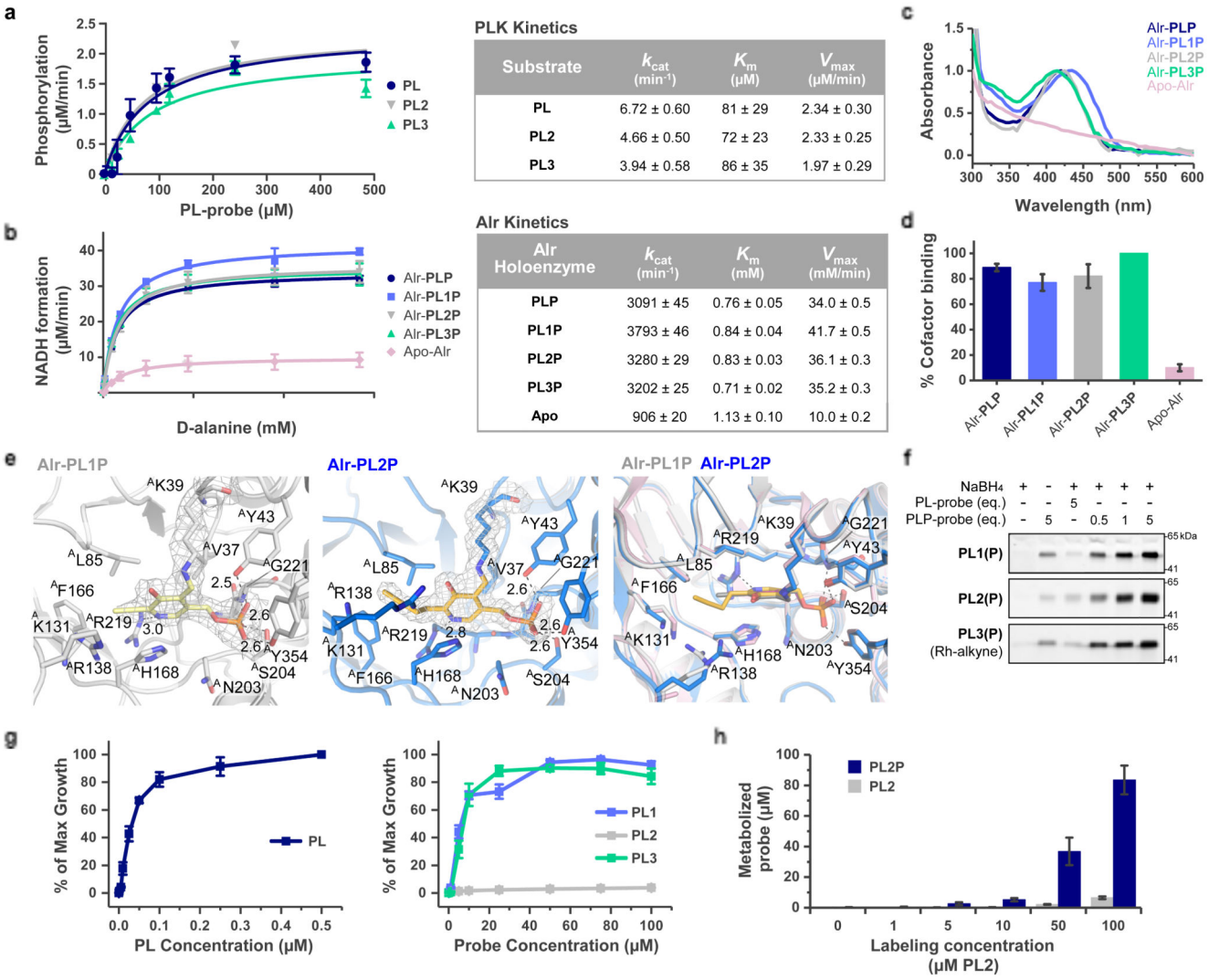

Figure 2. Biochemical characterization of PL probes.

(**a**) Kinetics of probe phosphorylation by *S. aureus* PLK. (n = 4, error bars: mean ± standard deviation). Kinetic analysis of **PL1** (325 nm) was not possible due to significant spectral overlap with NADH (340 nm). (**b**) Kinetics of alanine racemization (D- to L-Ala direction) by *S. aureus* Alr holoenzymes (0.01 μM) containing PLP or cofactor analogues (n = 3, error bars: mean ± standard deviation). (**c**) UV-vis absorption spectra of different *S. aureus* Alr holoenzymes (100 μM). Data was normalized to absorbance of the internal aldimine (420-430 nm). (**d**) Percent of *S. aureus* Alr holoenzymes bound by PLP or cofactor analogues upon $NaBH_4$ reduction and measurement by intact protein MS (n = 3, error bars: mean ± standard deviation). (**e**) Crystal structure of *S. aureus* Alr bound to **PL1P** (left, PDB 6G58) and **PL2P** (center, PDB 6G59). Simulated annealing omit electron density map contoured at 2.5 σ. Superimposed active sites (right) of PLP-bound Alr (purple, PDB 4A3Q),28 Alr-**PL1P** (grey) and Alr-**PL2P** (blue). Residues lining the active site as well as the **PL1P** (grey) and **PL2P** (gold) cofactors are shown as stick-models; hydrogen bonds are drawn as dashed lines. (**f**) Fluorescence SDS-PAGE of *S. aureus* Alr (10 μM) labeling using

Europe PMC Funders Author Manuscripts

PLP-probes (0.5, 1, 5 equivalents) or unphosphorylated PL-probes (5 equivalents). Coomassie staining and full gels in Supplementary Fig. 4. (**g**) Growth curves of *S. aureus* USA300 TnPdxS (Nebraska transposon library)33 in defined, PL-free media supplemented with PL (left) or probes (right). Bacterial growth was measured (OD_{600}) after 24 h and data was obtained from three biological replicates (error bars: mean ± standard deviation). (**h**) *In situ* metabolism of **PL2** to **PL2P** in *S. aureus* USA300 TnPdxS under labeling conditions (100 μM for 2 h at 37°C), ($n = 3$, error bars: mean ± standard deviation).

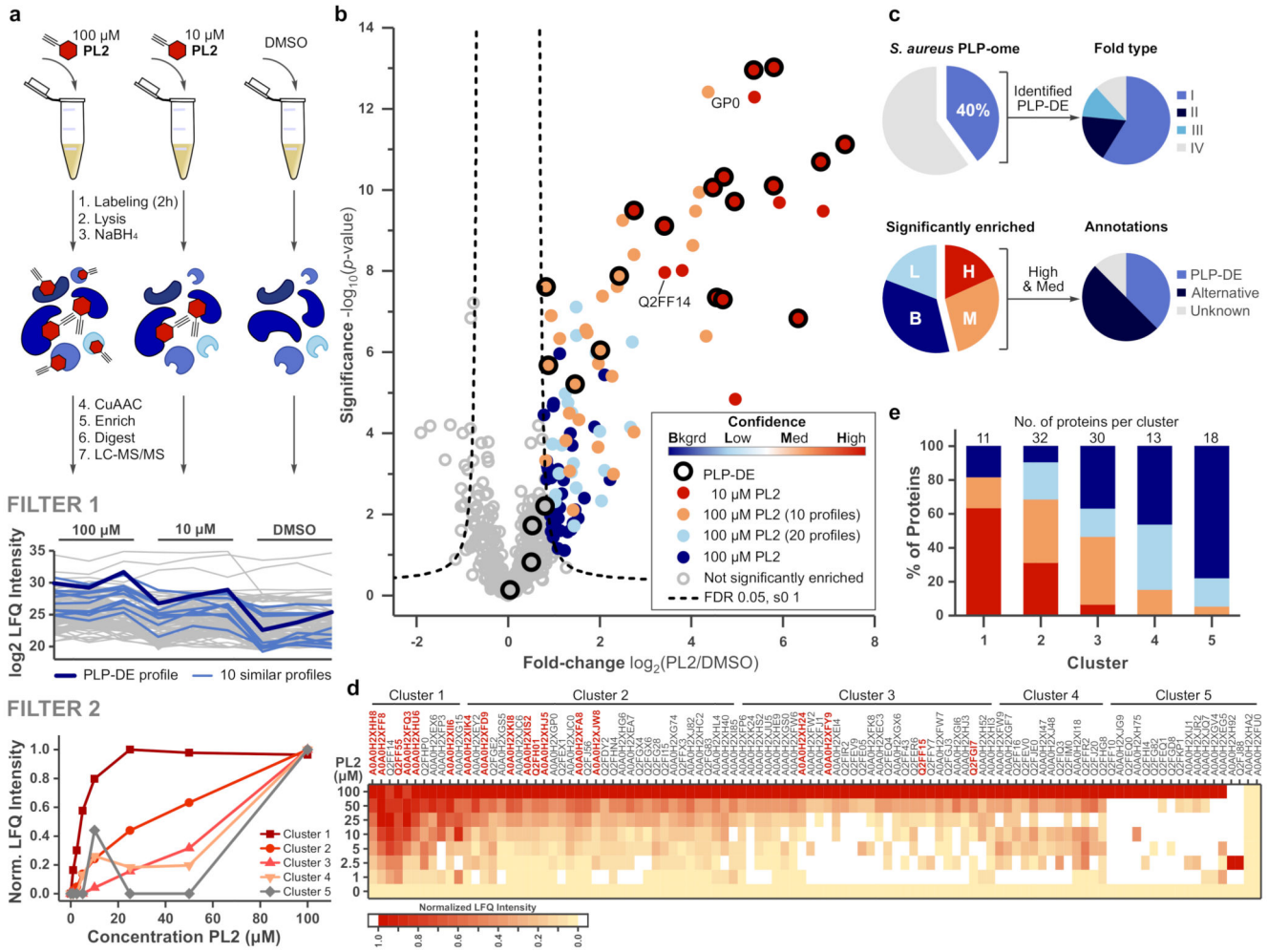

Figure 3. Proteomic profiling with PL2 shows significant enrichment of diverse PLP-DEs.

(**a**) Proteomic workflow and filtering strategy. *S. aureus* USA300 TnPdxS bacteria were labeled with **PL2** (100 and 10 µM) or DMSO (2 h). Upon cell lysis and $NaBH_4$ reduction, CuAAC to a biotin-azide tag enabled enrichment of labeled proteins, which were trypsin digested and subsequently analyzed by quantitative LC-MS/MS. Filter 1: LFQ-intensity profiles of enriched proteins were plotted and the 10 most similar profiles (Pearson correlation) of each PLP-DE were identified. Cysteine desulfurase (A0A0H2XHJ5) is shown as a representative example (dark blue). Filter 2: Proteomic experiments over eight concentrations reveals distinct binding behaviour of proteins, which were clustered (Pearson correlation) into 5 profile shape groups. Representative examples from each cluster are shown (bottom): Cluster 1 (A0A0H2XFF8), Cluster 2 (A0A0H2XFA8), Cluster 3 (A0A0H2XH24), Cluster 4 (Q2FF14), Cluster 5 (A0A0H2XH75). (**b**) Volcano plot visualization of fold-enrichment using 100 µM **PL2** compared to DMSO *versus* significance upon performing a two-sample t-test (FDR 0.05, s0 1; $n = 9$ biological replicates). Confidence levels determined by LFQ intensity profile searches are mapped by colour onto the plot: High (10 µM **PL2**, red), Medium (100 µM **PL2** + 10 profiles, orange), Low (100 µM **PL2** + 20 profiles, light blue), Background (100 µM **PL2**, dark blue), not significant

Europe PMC Funders Author Manuscripts

(grey). (**c**) (Top) Proportion of the *S. aureus* PLP-ome (40%) significantly identified in proteomic experiments and distribution of PLP-DE fold-types. (Bottom) Proportion of proteins in each confidence class and functional annotation of high- and medium-confidence proteins. (**d**) Heatmap representation of the mean LFQ intensities of significant proteins (from b) over several **PL2** concentrations (100, 50, 25, 10, 5, 2.5, 1, and 0 μM) performed as separate experiments (n = 3 biological replicates). Data were normalized to DMSO (= 0, light red) and absolute max binding (= 1, red) within individual protein datasets; proteins negatively enriched compared to DMSO (< 0) are shown in white. Proteins are labeled by their Uniprot ID and PLP-DEs are bolded in red. Clustering of proteins based on their LFQ-intensity profiles (Pearson correlation) is shown. See also Supplementary Fig. 9. (**e**) Percent of proteins from each confidence class per cluster. The number of proteins per cluster are written above each respective bar.

Europe PMC Funders Author Manuscripts

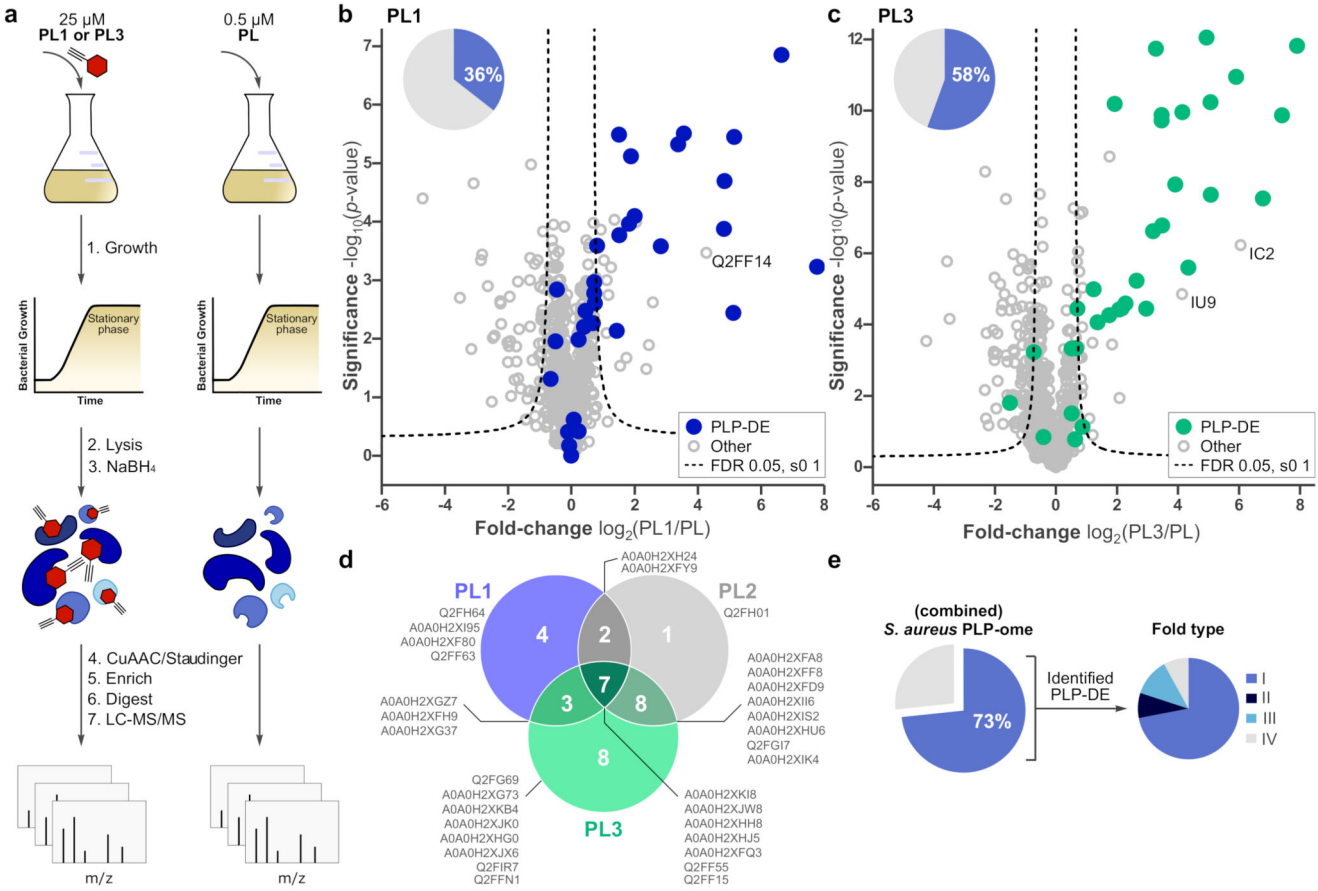

Figure 4. Growth medium supplementation with PL1 and PL3 probes enables broad PLP-ome coverage upon proteomic analysis.

(**a**) Proteomic workflow: *S. aureus* USA300 TnPdxS was grown to stationary phase in chemically-defined medium supplemented with **PL1** or **PL3** (25 µM) or PL (0.5 µM). After cell lysis and $NaBH_4$ reduction, samples were conjugated to a biotin tag via CuAAC (**PL1** experiment) or Staudinger ligation (**PL3** experiment). Labeled proteins were enriched, trypsin digested and analyzed by quantitative LC-MS/MS. (**b**) Volcano plot visualization of fold-enrichment of proteins upon labeling by growth media supplementation with **PL1** (25 µM) compared to PL (0.5 µM) *versus* significance upon performing a two-sample t-test (FDR 0.05, s0 1; $n = 3$ biological replicates). Significantly enriched proteins are listed in Supplementary Table 4. Inlay: Proportion of the *S. aureus* PLP-ome (36%) significantly identified in proteomic experiments. (**c**) Volcano plot visualization of fold-enrichment of proteins upon labeling by growth media supplementation with **PL3** (25 µM) compared to PL (0.5 µM) *versus* significance upon performing a two-sample t-test (FDR 0.05, s0 1; $n = 6$ biological replicates). Significantly enriched proteins are listed in Supplementary Table 5. Inlay: Proportion of the *S. aureus* PLP-ome (58%) significantly identified in proteomic experiments. (**d**) Venn diagram comparison of PLP-DEs (Uniprot ID) enriched using **PL1**, **PL2** and **PL3** in respective proteomic experiments. (**e**) Total proportion of the *S. aureus* PLP-ome (73%) significantly identified in proteomic experiments using **PL1**, **PL2** and **PL3** probes, and distribution of PLP-DE fold-types.

Europe PMC Funders Author Manuscripts

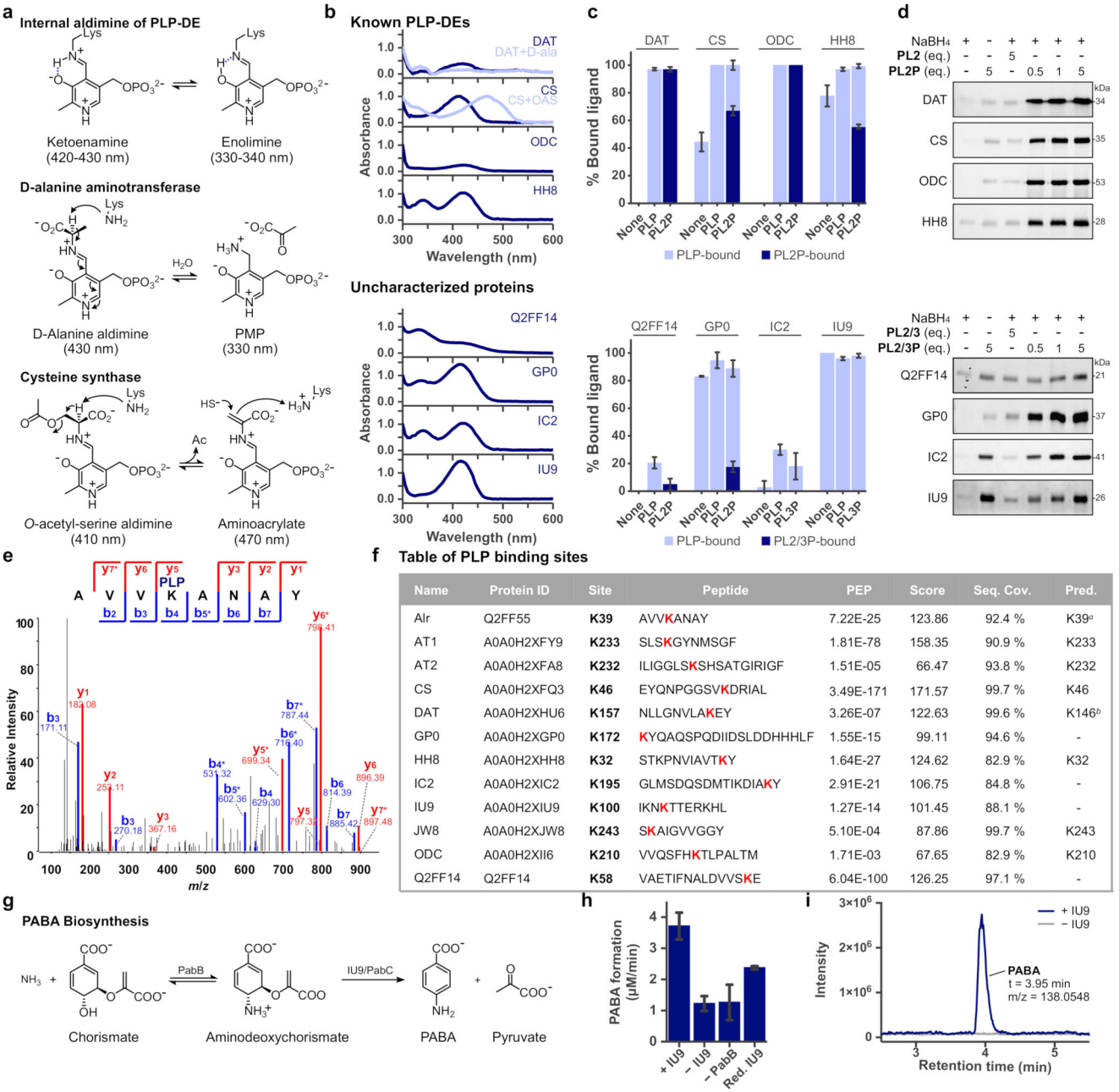

Name	Protein ID	Site	Peptide	PEP	Score	Seq. Cov.	Pred.
Alr	Q2FF55	**K39**	AVV**K**ANAY	7.22E-25	123.86	92.4 %	K39[a]
AT1	A0A0H2XFY9	**K233**	SLS**K**GYNMSGF	1.81E-78	158.35	90.9 %	K233
AT2	A0A0H2XFA8	**K232**	ILIGGLS**K**SHSATGIRIGF	1.51E-05	66.47	93.8 %	K232
CS	A0A0H2XFQ3	**K46**	EYQNPGGSV**K**DRIAL	3.49E-171	171.57	99.7 %	K46
DAT	A0A0H2XHU6	**K157**	NLLGNVLA**K**EY	3.26E-07	122.63	99.6 %	K146[b]
GP0	A0A0H2XGP0	**K172**	**K**YQAQSPQDIIDSLDDHHHLF	1.55E-15	99.11	94.6 %	-
HH8	A0A0H2XHH8	**K32**	STKPNVIAVT**K**Y	1.64E-27	124.62	82.9 %	K32
IC2	A0A0H2XIC2	**K195**	GLMSDQSDMTIKDIA**K**Y	2.91E-21	106.75	84.8 %	-
IU9	A0A0H2XIU9	**K100**	IKN**K**TTERKHL	1.27E-14	101.45	88.1 %	-
JW8	A0A0H2XJW8	**K243**	S**K**AIGVVGGY	5.10E-04	87.86	99.7 %	K243
ODC	A0A0H2XII6	**K210**	VVQSFH**K**TLPALTM	1.71E-03	67.65	82.9 %	K210
Q2FF14	Q2FF14	**K58**	VAETIFNALDVVS**K**E	6.04E-100	126.25	97.1 %	-

Figure 5. Validation of known and uncharacterized PLP-DE by UV-vis, MS and gel-based analysis.

(**a**) Characteristic spectral properties of PLP intermediates during enzyme catalysis.27,38 (**b**) UV-vis spectra of known PLP-DEs (top) and uncharacterized proteins (bottom). DAT and CS were incubated with respective substrates (10 equivalents) to observe PMP and aminoacrylate formation. Curves were normalized to absorbance at 300 nm. Further examples of PLP-DEs and aminotransferase substrate preferences in Supplementary Fig. 10. (**c**) Proportion of known PLP-DEs (top) and uncharacterized proteins (bottom) bound upon incubation with PLP or cofactor analogues (4 equivalents), $NaBH_4$ reduction and

measurement by intact protein MS (n = 3, error bars: mean ± standard deviation). Minimal nonspecific addition was observed for CS (5.9% PL, and 0.7% **PL2**) and IU9 (4% 2-fold PLP addition) (see Supplementary Table 6), and HH8 experiments were performed using only 1 equivalent of cofactor. (**d**) Fluorescence SDS-PAGE showing labeling of known PLP-DEs (top) and uncharacterized proteins (bottom) using **PL2P** or **PL3P** (0.5, 1, 5 equivalents) and **PL2** or **PL3** (5 equivalents) as a negative control, upon $NaBH_4$ reduction and CuAAC with rhodamine azide (**PL2**-based samples) or rhodamine alkyne (**PL3**-based samples). Coomassie staining and full gels in Supplementary Fig. 11. (**e**) Sample MS/MS spectrum (MaxQuant) for the PLP binding site peptide of Alr (Lys39). All other spectra in Supplementary Fig. 14. (**f**) Table of highest confidence PLP binding sites for known and uncharacterized proteins. PEP = posterior error probability (MaxQuant). Seq. Cov. = protein sequence coverage. Predicted sites were obtained using InterPro;39 [a]known site;28 [b]predicted site K146 was measured as unmodified. See detailed table in supporting information. (**g**) Biosynthesis of *p*-aminobenzoic acid (PABA) from chorismate by the enzymes aminodeoxychorismate synthase (PabB) and aminodeoxychorismate lyase (PabC). (**h**) Rate of PABA formation (μM/min) by IU9 (1 μM) in the presence of EcPabB (10 μM), chorismate (1 mM) and ammonium sulfate (50 mM), (n = 3, error bars: mean ± standard deviation). Inactive IU9 was prepared by $NaBH_4$ reduction of the PLP-bound internal aldimine. (**i**) Full scan LC-MS trace of PABA formation (rt: 3.95 min, $[M+H]^+$ 138.0548) under the above assay conditions following PABA extraction in EtOAc.

Europe PMC Funders Author Manuscripts

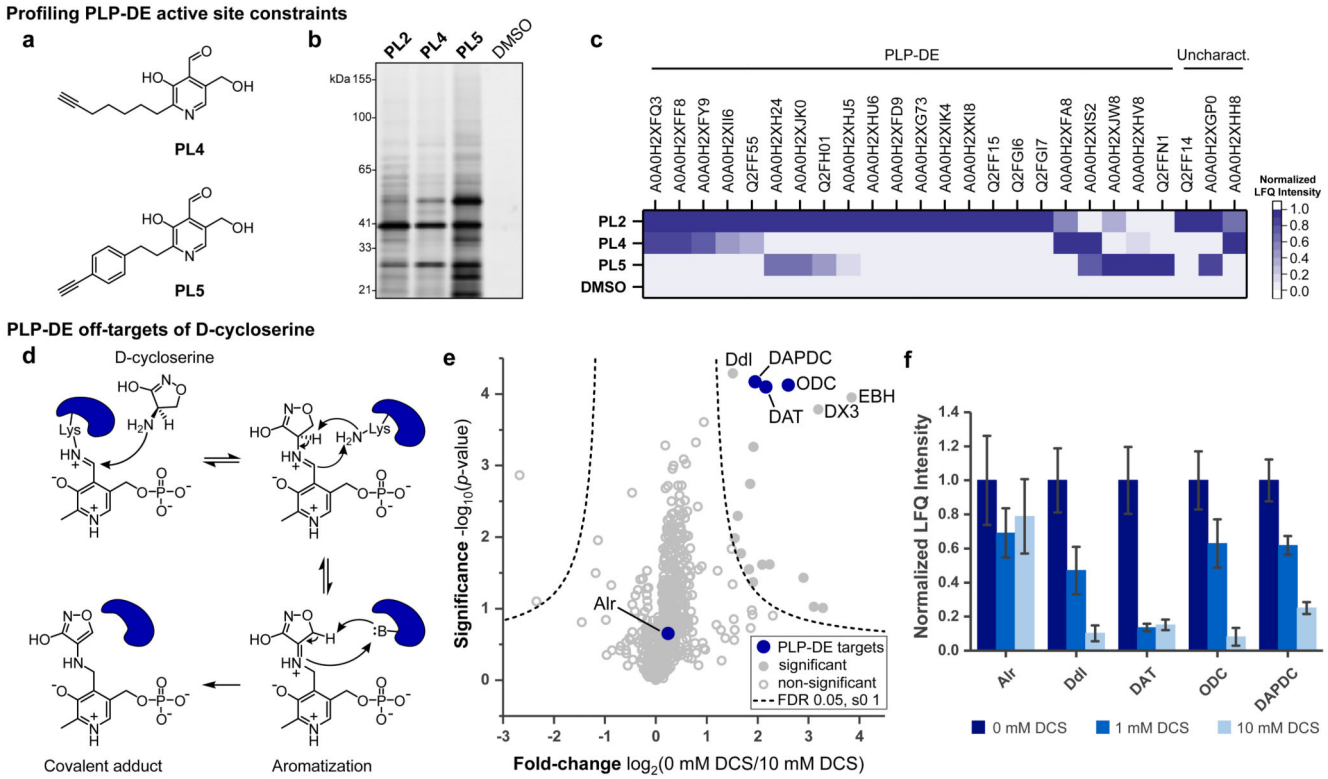

Figure 6. Applications of the PLP labeling method for profiling structural accommodation within PLP-binding sites and identifying PLP-DE off-targets of D-cycloserine.

(**a**) Chemical structures of **PL4** and **PL5** probes bearing extended bulk at the 2-methyl position of the PL-scaffold. (**b**) Fluorescence SDS-PAGE showing labeling of **PL4** and **PL5** (100 μM each) compared to **PL2** in *S. aureus* USA300 TnPdxS upon avidin-bead enrichment via trifunctional rhodamine-biotin-azide tag. (**c**) Heatmap representation of proteomic data ($n = 6$ biological replicates) showing normalized LFQ intensities of PLP-DEs and uncharacterized proteins identified. See Supplementary Fig. 16 for corresponding volcano plots and list of significant proteins (Supplementary Table 7). (**d**) Mechanism of DCS inhibition by formation of a stable aromatic PLP adduct within enzyme pockets. (**e**) Volcano plot showing competition of **PL2P** binding by DCS (10 mM) ($n = 3$ biological replicates). Proteins with highly significant fold-change between the two samples are labeled (EBH, Extracellular matrix binding protein (Q2FH04); DX3, Uncharacterized protein (A0A0H2XDX3)). Full list of significant proteins in Supplementary Table 8. (**f**) Normalized LFQ intensities of select DCS targets from proteomic data (10 and 1 mM DCS). Mean raw LFQ intensities were normalized to DMSO (= 0) and max intensity (= 1) within individual protein sets (error bars: mean ± s.e.m.).

Europe PMC Funders Author Manuscripts

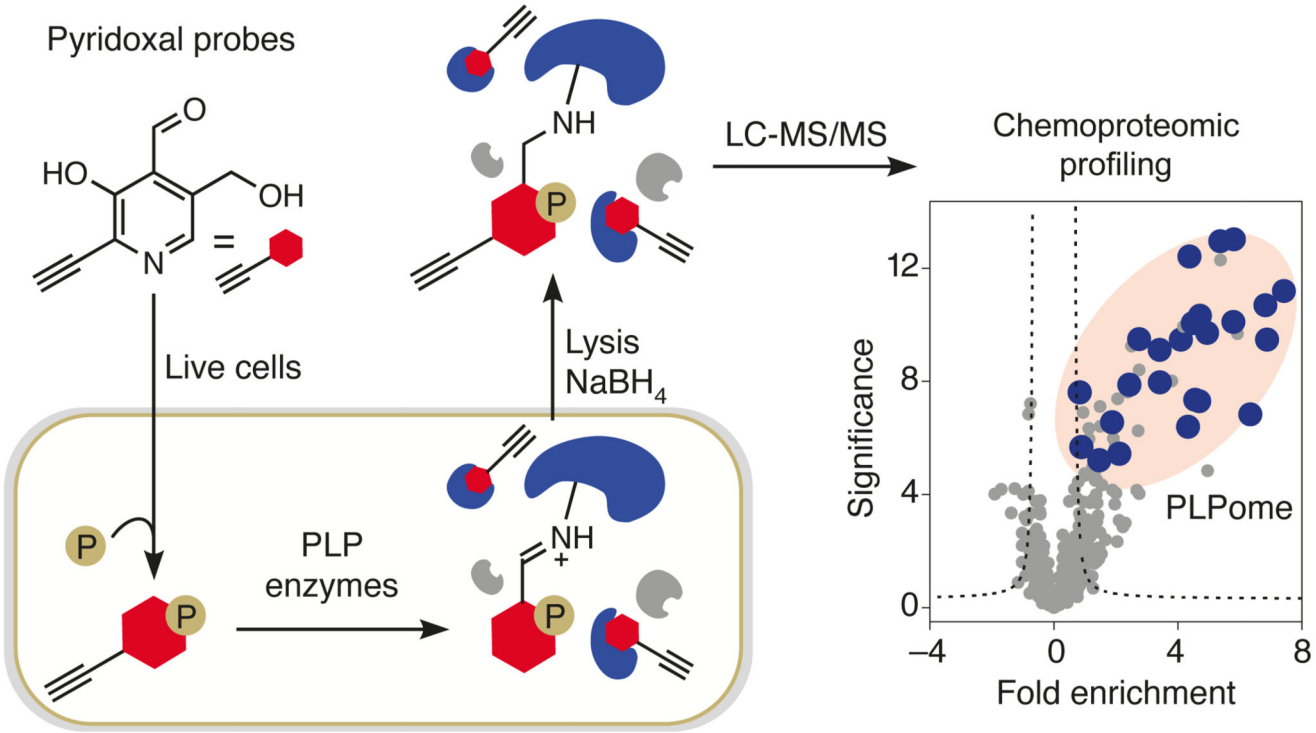

Europe PMC Funders Author Manuscripts

Europe PMC Funders Author Manuscripts

Table 1

PLP-DEs and select proteins of interest identified in Fig. 3b. Remaining proteins are listed in Supplementary Table 1. (Red = High confidence, Orange = Medium confidence, Grey = Non-significant).

		Fold-change	Significance	Name	Uniprot ID	Cluster
PLP-DE	1.	7.36	11.12	Cystathionine gamma-synthase (EC 4.4.1.8)	A0A0H2XFF8	1
	2.	6.82	10.69	Diaminopimelate decarboxylase (EC 4.1.1.20)	A0A0H2XFD9	2
	3.	6.34	6.83	Cysteine desulfurase (EC 2.8.1.7)	A0A0H2XHJ5	2
	4.	5.81	13.02	Cysteine synthase (EC 2.5.1.47)	A0A0H2XFQ3	1
	5.	5.79	10.10	Aminotransferase, class I (EC 2.6.1.-)	A0A0H2XFA8	2
	6.	5.37	12.96	Threonine synthase (EC 4.2.3.1)	A0A0H2XH24	3
	7.	4.94	9.71	Orn/Lys/Arg decarboxylase (EC 4.1.1.18)	A0A0H2XII6	1
	8.	4.71	10.32	Aminotransferase, class V	A0A0H2XKI8	2
	9.	4.69	7.29	L-threonine dehydratase catabolic TdcB (EC 4.3.1.19)	Q2FH01	2
	10.	4.56	7.34	Uncharacterized protein	A0A0H2XHH8	1
	11.	4.48	10.06	Branched-chain-amino-acid aminotransferase (EC 2.6.1.42)	A0A0H2XIS2	2
	12.	3.41	9.11	D-alanine aminotransferase (EC 2.6.1.21)	A0A0H2XHU6	1
	13.	2.75	9.49	Alanine racemase (EC 5.1.1.1)	Q2FF55	1
	14.	2.43	7.88	Aminotransferase, class I (EC 2.6.1.-)	A0A0H2XFY9	3
	15.	2.01	6.04	Probable glycine dehydrogenase subunit 2 (EC 1.4.4.2)	Q2FGI7	3
	16.	1.46	5.21	Serine hydroxymethyltransferase (EC 2.1.2.1)	Q2FF15	3
	17.	0.89	5.68	Ornithine aminotransferase (EC 2.6.1.13)	A0A0H2XIK4	2
	18.	0.83	7.61	Putative pyridoxal phosphate-dependent acyltransferase	A0A0H2XJW8	2
	19.	0.81	2.20	Probable glycine dehydrogenase subunit 1 (EC 1.4.4.2)	Q2FGI6	
	20.	0.53	1.72	Aminotransferase	A0A0H2XJK0	
	21.	0.51	0.82	Cysteine synthase/cystathionine beta-synthase (EC 2.5.1.47)	A0A0H2XG73	
	22.	0.04	0.13	Glutamate-1-semialdehyde 2,1-aminomutase 1 (EC 5.4.3.8)	Q2FG69	
Other	23.	6.88	9.47	Pseudouridine-5'-phosphate glycosidase (EC 4.2.1.70)	A0A0H2XJC6	2
	24.	5.92	9.69	Mevalonate kinase (EC 2.7.1.36)	A0A0H2XHE9	3
	25.	5.38	12.29	Putative heme-dependent peroxidase (EC 1.11.1.-)	Q2FJ56	2
	26.	4.96	4.83	Ferrochelatase (EC 4.99.1.1)	A0A0H2XGS5	2
	27.	3.81	8.02	Glutamyl-aminopeptidase (EC 3.4.11.7)	A0A0H2XJ82	2
	28.	3.42	7.96	UPF0340 protein SAUSA300_2068	Q2FF14	1
	29.	4.37	12.41	Uncharacterized protein	A0A0H2XGP0	2
	30.	4.33	6.39	Phosphopantothenoylcysteine decarboxylase (EC 4.1.1.36)	A0A0H2XFW7	3
	31.	1.55	4.33	D-alanine-D-alanine ligase (EC 6.3.2.4)	Q2FF43	3